Rewiring Dynamics of Functional Connectomes during Motor-Skill Learning

Saber Meamardoost, Mahasweta Bhattacharya, Eun Jung Hwang, Chi Ren, Linbing Wang, Claudia Mewes, Ying Zhang, Takaki Komiyama & Rudiyanto Gunawan

View supplementary material

Published online: 05 Oct 2023.

Submit your article to this journal

Article views: 1601
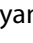
View related articles

View Crossmark data

Taylor & Francis
Taylor & Francis Group

Rewiring Dynamics of Functional Connectomes during Motor-Skill Learning

Saber Meamardoost[a] 🔟, Mahasweta Bhattacharya[b] 🔟, Eun Jung Hwang[c,d] 🔟, Chi Ren[c] 🔟, Linbing Wang[e] 🔟, Claudia Mewes[f], Ying Zhang[g] 🔟, Takaki Komiyama[c] 🔟, and Rudiyanto Gunawan[a] 🔟

[a]Department of Chemical and Biological Engineering, University at Buffalo, Buffalo, NY, USA; [b]Department of Biomedical Engineering, University at Buffalo, Buffalo, NY, USA; [c]Neurobiology Section, Center for Neural Circuits and Behavior, and Department of Neurosciences, University of California San Diego, La Jolla, CA, USA; [d]Cell Biology and Anatomy Discipline, Center for Brain Function and Repair, Chicago Medical School, Rosalind Franklin University of Medicine and Science, North Chicago, IL, USA; [e]Department of Civil and Environmental Engineering, Virginia Polytechnic Institute and State University, Blacksburg, VA, USA; [f]Department of Physics and Astronomy, University of Alabama, Tuscaloosa, AL, USA; [g]Department of Cell and Molecular Biology, University of Rhode Island, Kingston, RI, USA

ABSTRACT

The brain's functional connectome continually rewires throughout an organism's life. In this study, we sought to elucidate the operational principles of such rewiring in mouse primary motor cortex (M1) by analyzing calcium imaging of layer 2/3 (L2/3) and layer 5 (L5) neuronal activity in M1 of awake mice during a lever-press task learning. Our results show that L2/3 and L5 functional connectomes follow a similar learning-induced rewiring trajectory. More specifically, the connectomes rewire in a biphasic manner, where functional connectivity increases over the first few learning sessions, and then, it is gradually pruned to return to a homeostatic level of network density. We demonstrated that the increase of network connectivity in L2/3 connectomes, but not in L5, generates neuronal co-firing activity that correlates with improved motor performance (shorter cue-to-reward time), while motor performance remains relatively stable throughout the pruning phase. The results show a biphasic rewiring principle that involves the maximization of reward/performance and maintenance of network density. Finally, we demonstrated that the connectome rewiring in L2/3 is clustered around a core set of movement-associated neurons that form a highly interconnected hub in the connectomes, and that the activity of these core neurons stably encodes movement throughout learning.

1. Introduction

The brain's functional connectome—the functional connectivity of neurons—is the foundation of its myriad functions. This connectome is not static; quite the opposite, it continues to rewire throughout an organism's life (Citri and Malenka 2008; Bassett et al. 2011; Caroni et al. 2012; Bennett et al. 2018; Papale and Hooks 2018; Kao et al. 2020). Such plasticity is critical in enabling organisms to learn new skills, store new memory, and adapt and respond appropriately to novel environment (Bassett et al. 2011; Caroni et al. 2012; Papale and Hooks 2018; Kao et al. 2020). By unraveling the underlying principles governing the rewiring of the brain's functional connectome, we will be able to not only enhance our understanding of neurological disorders but also pave the way for developing innovative data storage paradigms and computing architectures (Bathe et al. 2021).

The primary motor cortex M1 is a hub for motor-skill learning and movement executions (Lee et al. 2022). M1 comprises multiple neuronal subtypes that are organized in layers (L1, L2/3, L4, L5 and L6), each with distinct

molecular markers, projections, and functions (Muñoz-Castañeda et al. 2021; Lee et al. 2022). It is generally thought that L2/3 is primarily involved in local processing, integrating sensory information with motor commands, and coordinating motor outputs, while L5 is responsible for generating motor commands and transmitting them to subcortical structures including the spinal cord, playing a direct role in the execution of motor movements. Connectome plasticity in M1 related to motor skill learning have been reported in both L2/3 and L5 (Greenough et al. 1985; Withers and Greenough 1989; Wang et al. 2011). However, the pattern of neuronal ensemble activity that evolves during motor learning differs between L2/3 and L5, suggesting that the two layers might exhibit distinct connectome plasticity (Peters et al. 2014; Peters et al. 2017).

Connectome plasticity occurs through the formation and degradation of synaptic connectivity between pre- and post-synaptic neurons, and the associated appearance and disappearance of dendritic spines (Fu et al. 2012; Peters et al. 2014; Huang et al. 2020; Albarran et al. 2021). Spine

formation has been observed across a variety of motor learning tasks (Papale and Hooks 2018) such as reaching and grasping (Xu et al. 2009), lever-pressing (Peters et al. 2014), and running on an accelerated motorized rod (Yang et al. 2009), across M1 layers, including L2/3 (Peters et al. 2014) and L5 (Xu et al. 2009; Yang et al. 2009).

Progress has been made in understanding how the functional circuitry of brain regions reconfigures during learning (e.g. using functional MRI (fMRI) data (Bassett et al. 2011; Kao et al. 2020)). Still, the principles behind functional rewiring among neurons are much less understood. Recent advances in neural activity recordings, such as two-photon (2 P) calcium imaging (Stosiek et al. 2003), have produced large-scale activity data of single neurons in awake animals while learning various tasks (Peters et al. 2014, 2017), opening the avenue to study brain's functional connectome at neuronal population level.

This work leverages large datasets of neuronal activities from L2/3 and L5 of M1 of mice during a lever-press task learning (Peters et al. 2014, 2017) for elucidating how functional connectomes in these regions are rewired during a motor-task learning and what operational objective(s) drives the connectome rewiring. To this end, we used the partial correlations of spiking activities, inferred from 2 P calcium imaging, between any pair of neurons as a measure of their functional connectivity. We analyzed how functional connectomes in L2/3 and L5 of M1 rewire during learning and how this rewiring is associated with motor performance. We then studied the rewiring of functional connectivity among neurons that are most impacted by learning and identified groups of neurons that have different learning-induced rewiring patterns. Our results show that the functional connectomes in both layers continually rewire throughout the learning period following a common trajectory where connectomes transiently increase their functional connections before returning to a homeostatic level of connectivity. Further, we observed the existence of an interconnected hub of movement-associated neurons in the connectomes that are heavily rewired and stably encode movement during learning.

2. Materials and Methods

2.1. Animals

Two groups of mice were used in this work from two separate studies previously published where neuronal activity in L2/3 (Peters et al. 2014) and L5 (Peters et al. 2017) was recorded during learning a lever-press task. These animals are referred to as L2/3 ($n = 7$) and L5 ($n = 8$) mice corresponding to the cortical layer of neurons from each mouse. The number of neurons N recorded from each animal and layer is provided in Table S1. Note that one animal (Mouse L2/3-6) was removed from the analyses due to multiple missing sessions of training.

2.2. Experiments: Lever-Press Task

Details on experimental procedure and data collection are available in the original publication (Peters et al. 2014,

2017). Briefly, genetically encoded calcium indicator (GCaMP5G or GCaMP6f) was virally expressed in the motor cortex of mice (C57BL/6). In the experiments, water deprived head-fixed mice performed a lever-press task learning. In the task, the mice learned to press a lever beyond a set threshold (~ 3 mm) using their left forelimb within 10–30 s after an auditory tone was presented to receive a water droplet as reward (see Figure 2a). Calcium fluorescence images of L2/3 and L5 neuronal activity were recorded at ~ 28 Hz using 2 P microscopy, from the same field of view—for L2/3, an area of 472 μm× 508 μm of the right forelimb of the motor cortex (Peters et al. 2014) and for L5, an area of 340 μm× 340 μm of the apical corticospinal dendrites of the motor cortex (Peters et al. 2017)—across 14 learning sessions (1 session/day; 20–30 min/session). Meanwhile, lever displacement trace was recorded at 10 kHz. Regions of interest (ROIs) in the calcium images were manually drawn to demarcate the somas or dendritic shafts of individual single neurons and then, aligned across sessions. Pixels within each ROI were averaged, and background fluorescence fluctuations were subtracted from the average before calculating a calcium fluorescence time series (dF/F) for each neuron.

2.3. Functional connectome inference

Functional connectomes were inferred from 2p calcium fluorescence imaging data using FARCI, a recently developed connectome inference pipeline (Meamardoost et al. 2021). Briefly, the input to FARCI is calcium time-series dF/F data. FARCI uses Online Active Set method to Infer Spikes (OASIS) algorithm (Friedrich et al. 2017) from the Suite2p package (Pachitariu et al. 2018), to deconvolve neuronal spiking activity from 2p calcium imaging data. Subsequently, the deconvolved spikes are thresholded to keep only significant calcium spikes (larger than $\mu + 2\sigma$) and then, smoothened using a moving window weighted average (5 frames) (Meamardoost et al. 2021). As described in the original FARCI publication, the preprocessing steps above were tuned to give robust and accurate functional connectivity. Finally, an $N \times N$ partial correlation matrix is generated where N represents the number of neurons. To produce the adjacency matrix of the functional connectome, we thresholded the partial correlations, keeping only those that are larger than $\mu + 2\sigma$ in each session. Each element in this $N \times N$ adjacency matrix represents the functional connectivity between two corresponding neurons, and each pair of neurons forms an edge in the connectome.

2.4. Functional connectome rewiring

To study the dynamics of connectome rewiring over multiple sessions of motor skill learning, the functional connectome inference as described above was applied to the neuronal activity data collected from different sessions separately. This step generated an ($N \times N$) adjacency matrix. Note that the number of neurons N differs across mice (see Table S1). The upper triangular part of this matrix was extracted and stored as a single-row adjacency vector

containing $\frac{N(N-1)}{2}$ elements. The adjacency vectors from different sessions were then stacked to give a matrix with $\frac{N(N-1)}{2}$ columns and s rows, where s is the number of learning sessions. Finally, Principal Component Analysis (PCA) was applied to this matrix—each row vector from a session represents an observation, while each column vector (partial correlation between two neurons) is a feature. The PC scores were used to visualize the connectome rewiring dynamics during motor skill learning. To check whether our results are consistent across different dimensionality reduction methods, we also applied Multidimensional Scaling (MDS) (Anon 1987) and Uniform Manifold Approximation and Projection (UMAP) (McInnes et al. 2020) to the functional connectome matrix above.

2.5. Trial-Based Functional Connectome Activity

To evaluate the activity of functional connectome on a single trial basis, we first extracted smoothened calcium spikes from movement-related frames in the respective session, as illustrated in Figure 1a. We applied FARCI to generate movement-related functional connectome for the learning session. The adjacency matrix of this connectome was then binarized—partial coefficients that are larger than $\mu + 2\sigma$ are set to 1, and otherwise 0. Separately, we extracted smoothened calcium spikes for each rewarded trial and evaluated pairwise Pearson's correlations for all neuron pairs to produce a correlation matrix (see Figure 1b). Finally, we computed the Hadamard product of the Pearson correlation matrix of a trial and the binarized adjacency matrix of movement-related functional connectome of the session, to give trial-based activity of the connectome (see Figure 1c). Following the visualization of functional connectome rewiring above, we extracted the upper triangular part of the resulting connectome activity matrices and applied PCA to obtain a reduced dimensional visualization.

2.6. Time-Series PCA

Time-series PCA was applied to project neuronal population activity during rewarded trials to a lower dimensional space (Sauerbrei et al. 2020). To do so, for each rewarded trial, we identified the frame corresponding to movement onset (see Figure 1b) and extracted smoothened calcium spikes from a 98-frame time window that was defined such that the movement onset is the 15-th frame in this window. Then, we converted the smoothened calcium spikes of each neuron to z-scores by using their trial-based average and variance. These z-scores were then averaged across the trials in a session, to which PCA was applied—each time point was an observation and the average z-score of a neuron was a feature. The resulting principal components were then used to visualize the time-series neuronal activity as 3D trajectory in PC1-3 space. We applied the above procedure to calcium data from each session separately.

2.7. Network connectivity Analysis

We employed four different metrics: mean degree, network density, transitivity, and clustering coefficient, to characterize the interconnectedness of the functional connectomes. Mean degree is the average number of connections for a neuron. Meanwhile, network density gives the ratio of the number of connections (i.e. the number of non-zero elements in the adjacency matrix) and the total possible connections (i.e. N^2). Transitivity is computed as the ratio between the number of existing closed triplets in the connectome graph and the total possible number of triplets in a neuronal population. Finally, clustering coefficient is defined for each node (neuron) i as the ratio between the number of triangles connected to neuron i and the number of triplets centered on i. For a functional connectome, we evaluated the mean (average) clustering coefficient across all neurons. Both transitivity and clustering coefficients give a measure for the tendency of neurons to form clusters in the connectome. For all of the above metrics, a higher value indicates a more interconnected network.

2.8. Pseudotime analysis of Trial-Based Functional Connectome Activity

Trial-based functional connectome activities were computed and PCA was applied to the connectome activity matrices, as described above. Pseudotime analysis was performed using the method Diffusion PseudoTime (DPT) that was originally developed for reconstructing gene expression dynamics from static snapshot single-cell transcriptome data of cell differentiation (Haghverdi et al. 2016). DPT employs the diffusion map to organize data points into a nearest neighbor graph with weighted edges, based on which a transition matrix is generated. This transition matrix approximates the dynamic transitions across the data points, starting from a user-prescribed root, mimicking a random walk. We applied the DPT function in the Python package scanpy (Wolf et al. 2018), specifically using the 'umap' kernel function for neighborhood graph, with the default parameters (number of neighbors, n_neighbors = 15 and number of diffusion component, n_dcs = 10). Each trial was represented by its PC scores, the number of which was determined so that the cumulative explained variance reached 95% of the total variance. The first trial from the first session was assigned to be the root node that corresponds to the pseudotime of 0. Finally, Pearson correlations between the cue-to-reward time and pseudotime were computed for Sessions 1–4 (first phase) and Sessions 5–14 (second phase) of learning. To establish the statistical significance, Fisher z-transformation was first applied to the correlations (Fisher 1921) and then, a two-sided two-sample t-test was applied to their difference.

2.9. Classification and Analysis of Movement-Related Neurons

We followed the procedure outlined in the original publication to classify neurons as 'movement-related' (Peters et al. 2014).
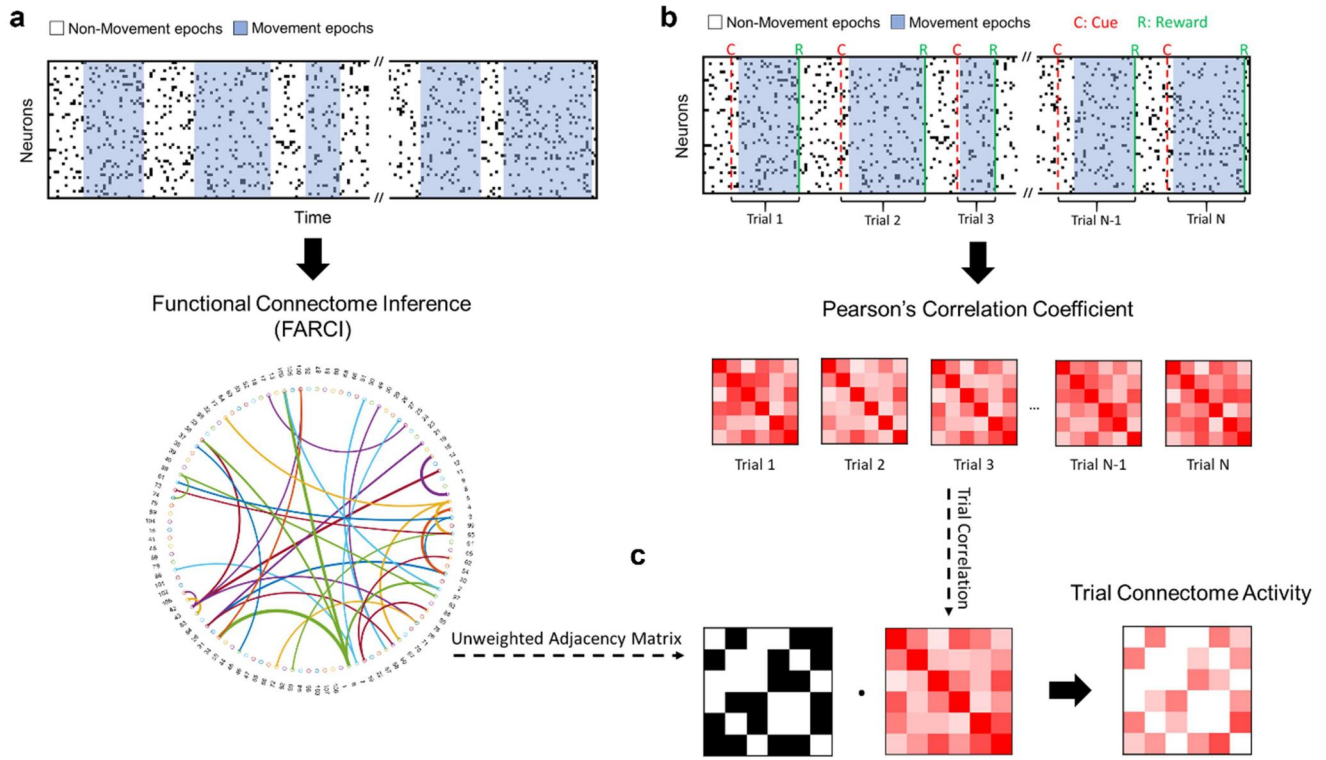
Figure 1. Data processing for the inference of functional connectome and trial connectome activity. **a.** Functional connectome inference pipeline. For each session, FARCI is applied to produce the functional connectome. **b-c.** Trial-based connectome activity. Pairwise Pearson's correlations are computed using the activities of neuron pairs for a rewarded trial (cue-to-reward), which are then filtered using a binary adjacency matrix obtained from functional connectome, to give the connectome activity of the trial.

The classification was performed based on the level of neuronal activity during movement epochs. Briefly, binarized lever traces were used to label the calcium fluorescence imaging frames into movement and quiescent epochs. The mean activity of each neuron was computed over the movement epochs in a session. Subsequently, the movement and quiescent epochs were shuffled, thereby randomizing the relative position of these epochs with each other. The mean activity of neurons for the shuffled epochs was computed in each shuffle, and this shuffling was repeated 10,000 times. A neuron was classified as movement related if its mean activity during the movement epochs was higher than the 0.5th percentile of the 10,000 mean activities computed for the randomly shuffled epochs.

To evaluate the fraction of movement related neurons in the edges that account for the largest connectome changes over learning, we first sorted edges based on their loadings to PC1 in the above PCA of functional connectome rewiring in descending order. Subsequently, we identified two groups: the highest 100 edges (top positive PC1 loadings) and the lowest 100 edges (top negative PC1 loading). For each group, we compiled neurons that are incident these edges—two for every edge–resulting in a set of 200 non-unique neurons for each group. For each neuron in these groups, we calculated the number of times that it was classified as movement-related across different periods of learning: sessions 1–2, 3–5, 6–9, and 10–14. The fraction of movement-related neurons was computed by dividing the total number of times that the top PC1 neurons are classified as movement-related with the total number of neurons multiplied by the number of sessions in the learning period (i.e. 200 x m, where m is the number of sessions in a learning period. For example, for sessions 6--9, m is 4). To establish the significance level, we repeated the above procedure using 100 edges that are randomly sampled from the union of edges in the connectomes across all sessions, for a total of 1000 times. To establish statistical significance, we evaluated the kth upper percentile associated with the fraction of movement-related neurons for each learning period with respect to the distribution of the fraction from the random sampling of edges.

2.10. Evaluation of Session-to-Session Changes in Functional Connectivity

To assess the degree to which neurons change their connectivity during motor learning, we first computed functional connectome in each session and evaluated the number of connections that change between two consecutive sessions for each neuron. Next, for a given group of neurons, we computed the average session-to-session change in connectivity as the ratio of total number of altered connections across all the neurons to $n \times (s - 1)$ where n and s are the number of neurons and sessions, respectively.

2.11. Identification of Core, Naive Phase, Expert Phase, and Other Neurons

We classified neurons based on their connectivity changes into four types: Core, Naïve Phase (NP), Expert Phase (EP),
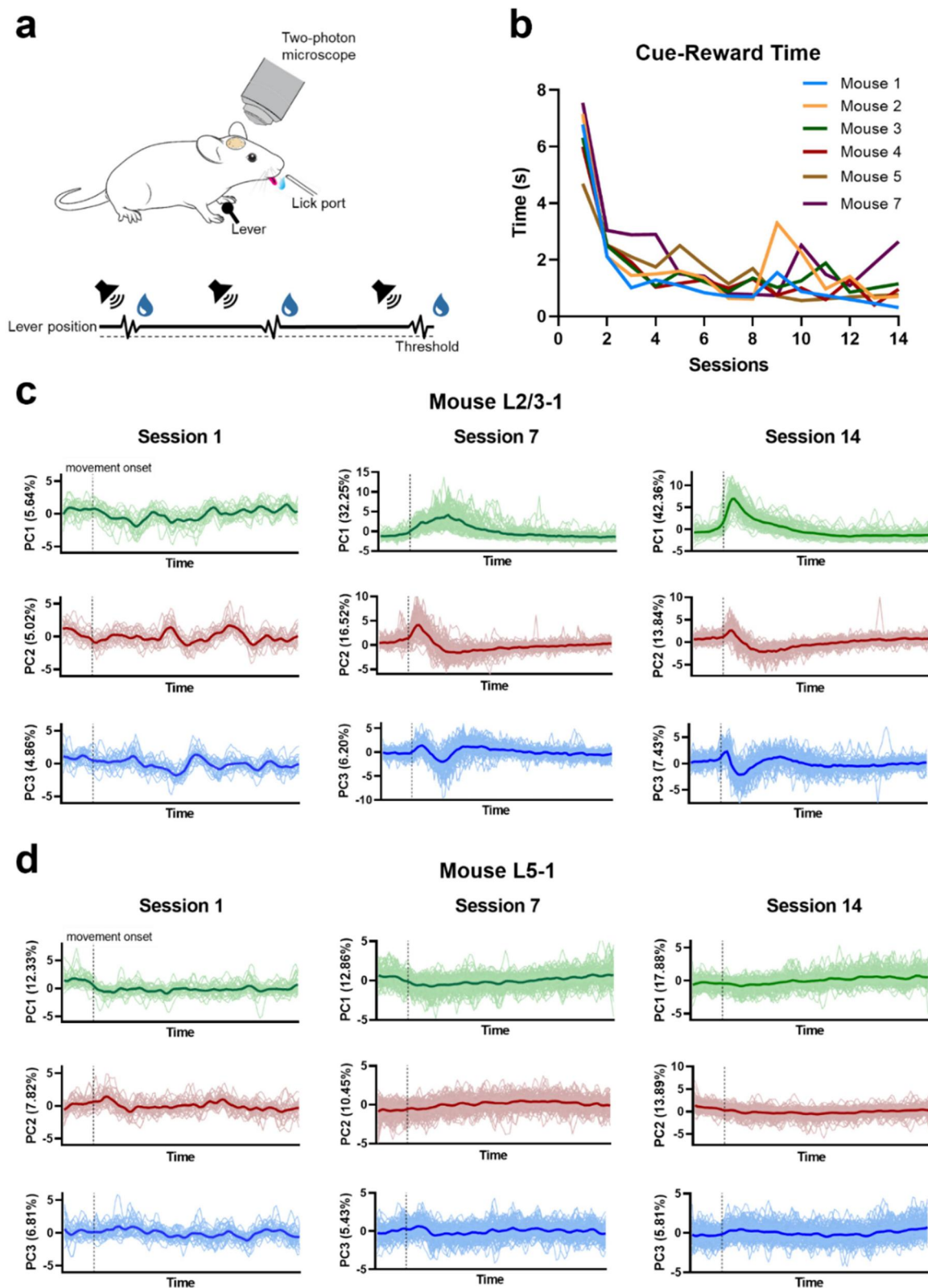
Figure 2. Neuronal population activity of L2/3 and L5 regions of primary motor cortex M1 in lever-press task learning. a. Lever-press task schematic. **b.** Mean duration between cue and reward, averaged across all rewarded trials from each session. **c, d.** Scores of the first three principal components (PCs) of neuronal population activity across sessions in L2/3 (Mouse L2/3-1) and L5 (Mouse L5-1) regions, respectively. Dark lines show the average values among trials. The neuronal population activities were extracted from a 98-frame window of every rewarded trial. The window was anchored by the movement onset time, which was set to be the 15th frame in this window. The green dot marks the starting time point.

and Other (O). The classification used the PCA of the functional connectomes described above. For each mouse, we determined the set of edges in the functional connectome that are associated with highly positive and negative PC1 loadings using a threshold determined by the knee detection algorithm (Satopaa et al. 2011). Then, we identified two sets

of neurons, one set that is incident to connectivity from the top positive PC1 loading and another to the top negative PC1 loadings. Neurons belonging to both sets are labelled as Core neurons. Those that are associated with only the top positive PC1 loadings are labeled as EP, while those associated with only the top negative PC1 loadings as NP. Neurons that are not in the three sets above are called Other (O) neurons.

2.12. Correlations with Expert (Learned) Activity and Movement Pattern

To examine the similarity of neural population activity in an individual trial to the learned expert activity or the similarity of movement to the learned movement pattern, we performed correlation analysis. Neuronal spiking activity data were preprocessed as above. The expert activity and movement patterns refer to the average activity and movement in 84-frame windows of rewarded trials over sessions 10-14. The first frame in this 84-frame window corresponds to the movement onset.

2.13. Linear Decoders of Neuronal Activity to Lever Position

To map neuronal activity to movement for each group of neurons, we used pre-processed neuronal spiking activity data as above. Rewarded trials in each session were then split randomly into train and test sets at 80% and 20% ratio, respectively. For a given session, a decoder was trained using linear regression (ordinary least square) to predict lever position (*i.e.* lever voltages) from the spike data of a specific set of neurons (Core, EP, NP, and O neurons). The performance of the trained linear decoder was then assessed by computing the correlations between the predicted and actual lever positions (measured in voltages) using data from the test set. In addition, an expert decoder was trained using the combined data from sessions 10–14, and its performance was tested on the data from sessions 1–3.

3. Results

3.1. Motor Skill Learning Reconfigures Functional Connectome in the Motor Cortex

Lever-press task learning experiments were previously carried out where water-deprived head-fixed mice ($n = 7$) learned to press a lever in response to an auditory cue in order to receive a water droplet reward. Neuronal activity from L2/3 or L5 of mouse primary motor cortex (M1) were recorded using 2p calcium imaging (see illustration in Figure 2a) (Peters et al. 2014, 2017). The average times between the cue and the corresponding reward decreased with learning (see Figure 2b), indicating that these mice were able to acquire reward increasingly more efficiently.

Lever-press task learning reshaped the neuronal activity in M1 L2/3 generating reproducible neuronal activity pattern and more consistent relationship between neuronal activity and movements (Peters et al. 2014). Time-series PCA of L2/3 neuronal activity in Figure 2c confirms the emergence of more consistent temporal activity pattern with learning (see Supplementary Figure S1–6 for the complete results) with increased synchronization of activity at or around the movement onset. In contrast, the activity of L5 corticospinal neurons did not become more consistent with learning. Rather, learning led to more dissimilar neuronal activity for dissimilar movements (Peters et al. 2017). In congruence with these observations, time-series PCA of L5 neuronal activity as shown in Figure 2d shows a lack of trial-to-trial coherence across the learning sessions (see Supplementary Figure S7–14 for the complete results). Thus, lever-press task learning induces distinct reorganizations of neuronal population activities and thus the functional connectome in different layers of M1.
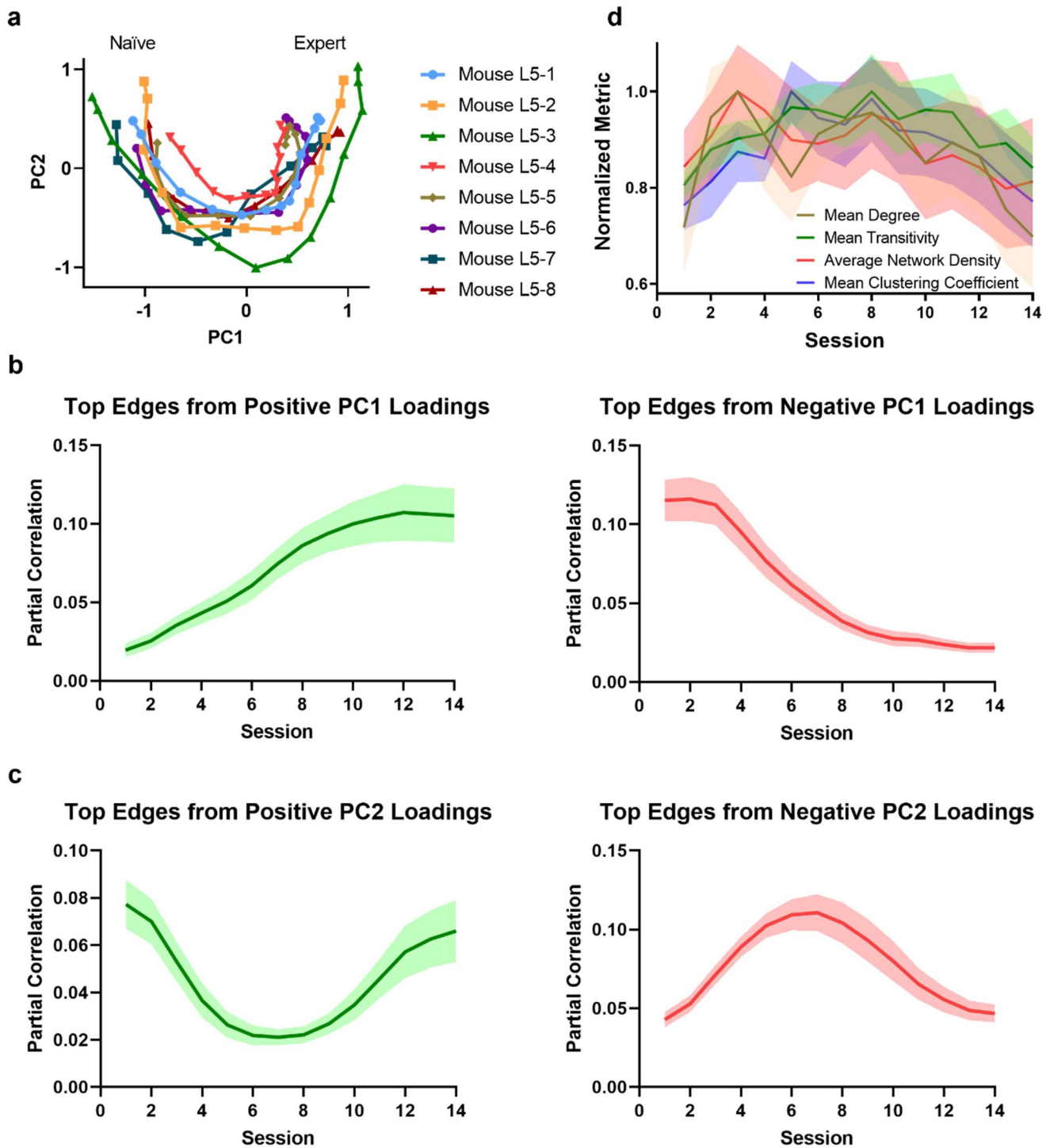
To study functional connectome rewiring dynamics associated with lever-press task learning, we used partial correlations of neuronal spikes, computed using a recent connectome inference method FARCI, to establish functional connectivity among excitatory neurons in L2/3 and in L5. Figure 3a displays L2/3 functional connectome rewiring, projected to the first two PC axes (see Methods), portraying homogeneous common trajectories for different animals (see Supplementary Figure S15 for individual mice using PCA). The similarities in the rewiring trajectories are not dependent on the thresholding of the partial correlations (see Supplementary Figure S16 for results without thresholding), nor on the dimensionality reduction technique since MDS (Anon 1987) and UMAP (McInnes et al. 2020) also generate rewiring trajectories that are similar among mice (see Supplementary Figure S17-18). The rewiring trajectories show that the strongest contributor to the functional connectome variation across sessions is associated with learning. The first two PCs together explain between 52% to 62% of the total variance (Supplementary Figure S15). Figure 3b–c illustrate the dynamics of the average partial correlations associated with the 100 most positive and most negative loadings from the first and second PCs (*i.e.* PC1 and PC2). The dynamics indicates the continuous (monotonous) gain or loss of functional connections along the PC1 axis, and transitory gain or loss of connections along the PC2 axis. Finally, Figure 3d illustrates the connectivity changes in the functional connectomes (mean degree, network density, transitivity, mean clustering coefficients) over the animals in the study, showing a sharp increase in the functional interconnectedness among neurons during the first 3–4 sessions, followed by a more gradual decrease in connectivity during the remaining sessions. The increase (decrease) in functional connectivity reflects the overall strengthening (weakening) of partial correlations of the neuronal firing activity. The results above suggest a common rewiring dynamics of L2/3 functional connectomes among the mice subjected to lever-press task learning, where the functional connectome quickly increases its degree of connectivity (increased co-firing among neurons) during the initial stages of learning and is then pruned to bring network interconnectedness toward the same level as that before learning.
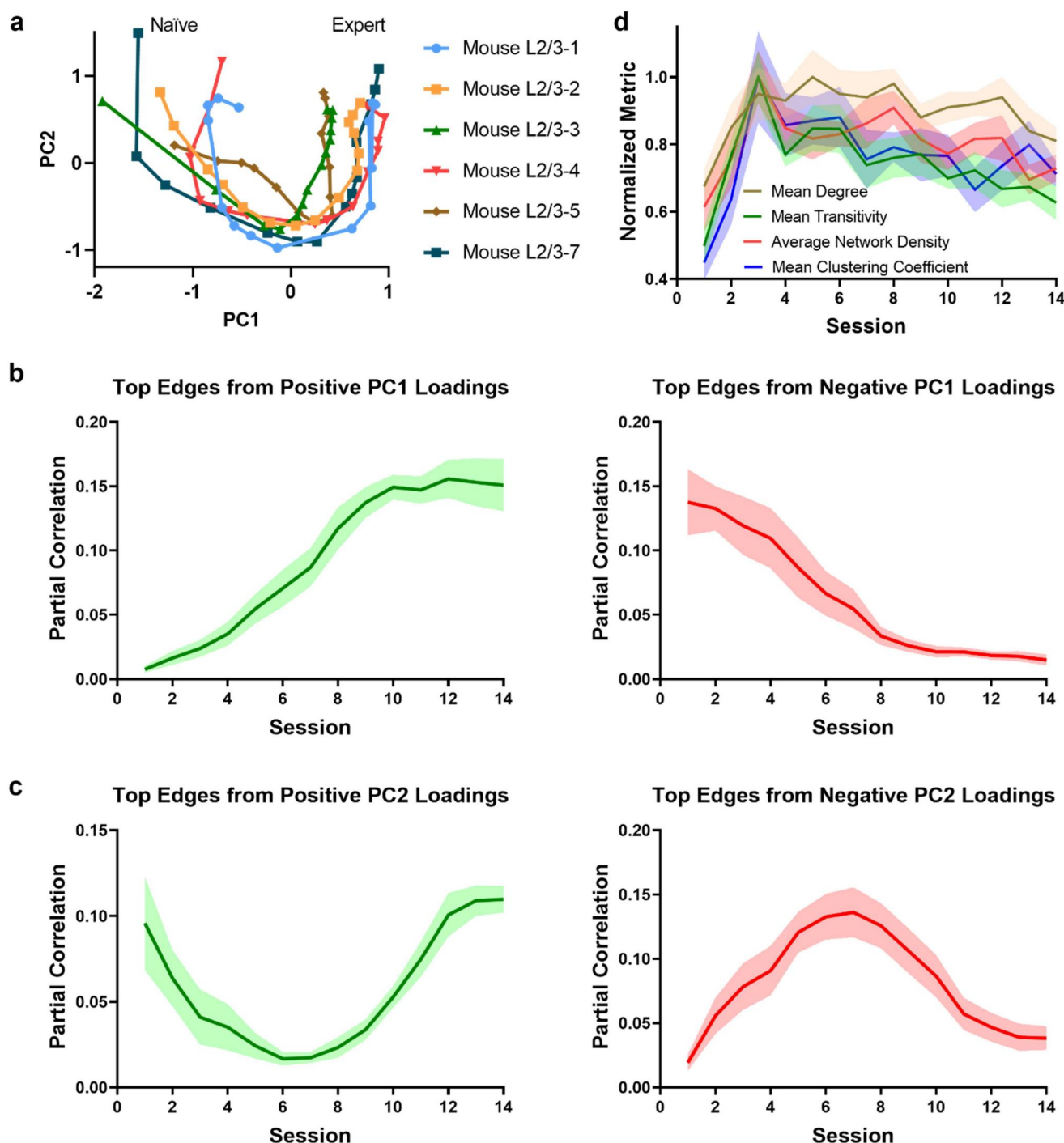
Figure 3. Functional connectome rewiring in L2/3 during lever-press task learning. The shaded areas indicate s.e.m., computed over the mice in the study. **a.** Connectome rewiring trajectories. Functional connectomes are projected onto PC1 and PC2 axes (see Methods). **b–c.** Average partial correlation coefficients of top 100 edges based on positive and negative magnitudes of PC1 and PC2 loadings. **d.** Network connectivity metrics of the functional connectomes. To aid comparison, normalized metrics are shown, using the highest value of each metric across sessions and animals as a scaling factor (see Supplementary Figure S24 for full results).

Figure 4a–c gives the functional connectome rewiring dynamics for L5 (see Supplementary Figure S19–21 for individual mice using PCA, MDS, and UMAP projection). Interestingly, despite the differences between L2/3 and L5 in how lever-press task learning alters neuronal activities, similar rewiring trajectories are observed across all mice in these layers. The first PC axis is again associated with the stable monotonous gain or loss of functional connections related to learning, while the second PC axis captures the transitory gain or loss of functional connections. The top two PCs cumulatively explain between 61% to 77% of the total variance among the connectomes from different sessions (Supplementary Figure S19). Figure 4d gives the dynamic changes in network interconnectedness for the functional connectomes in L5, showing similar dynamics, albeit more subdued and delayed when compared with those in L2/3. The similarities in the functional

Figure 4. Functional connectome rewiring in L5 during lever-press task learning. The shaded areas indicate s.e.m., computed over the mice in the study. **a.** Connectome rewiring trajectories. Functional connectomes are projected onto PC1 and PC2 axes (see Methods). **b–c.** Average partial correlation coefficients of top 100 edges based on positive and negative magnitudes of PC1 and PC2 loadings. **d.** Network connectivity measures of the functional connectomes. To aid comparison, normalized metrics are shown, using the highest value of each metric across sessions and animals as a scaling factor (see Supplementary Figure S25 for full results).

connectome rewiring dynamics between L2/3 and L5 suggest the existence of a common operating principle in M1.

3.2. Connectome Rewiring in Motor Cortex is a Biphasic Process

Next, we studied how functional connectome activity is related to motor task performance on a trial-by-trial basis. To this

end, we evaluated functional connectome activities using gated pairwise Pearson correlations of neuronal calcium spike activities in rewarded trials (see Methods), providing a measure for the co-firing activity of connected neurons. Figure 5 depicts the L2/3 functional connectome activities from rewarded trials in individual mice, and their associated cue-to-reward times. Expectedly, the functional connectome activities across sessions follow a similar trajectory in the PC1-PC2 projection

(*x-y* axes) to the rewiring dynamics shown above. We noted that the relationship between L2/3 functional connectome activity and task performance can be divided into two phases: in the first phase (up to session 3–4), alterations in the functional connectome activities are associated with a rapid improvement in motor performance leading to a sharp drop in the cue-to-reward time. In the subsequent phase, functional connectome activities continue to change while motor performance remains stable. Interestingly, as shown in Figure 3a & d, the first phase is marked by a sharp increase in the connectivity of the functional connectomes, while the second phase corresponds to a period of gradual pruning of the connectome. Figure 6 shows the L5 functional connectome activity and the motor performance for every rewarded trial from individual mice. Consistent with the key findings of the original study (Peters et al. 2017), the activity of L5 functional

connectomes has a weaker relationship with the motor performance in comparison with L2/3.

To establish the observed biphasic process more firmly, we evaluated the correlations between the cue-to-reward times and the learning-related trajectory of the functional connectome activities. For this purpose, we applied an analysis commonly used in single-cell studies, called pseudotime analysis, to the functional connectome activities (see Methods). Here, the pseudotimes reflected the progression of motor-skill learning, where the first trial of the first session was set to be the "root cell." The DPT method (see Methods) generated the pseudotime for each trial activity based on a random walk (diffusion), starting from the root (pseudotime = 0) and ending at the trial activity furthest away from the root (pseudotime = 1). The results of the pseudotime analysis for L2/3 and L5 are provided in Supplementary Figure S22.
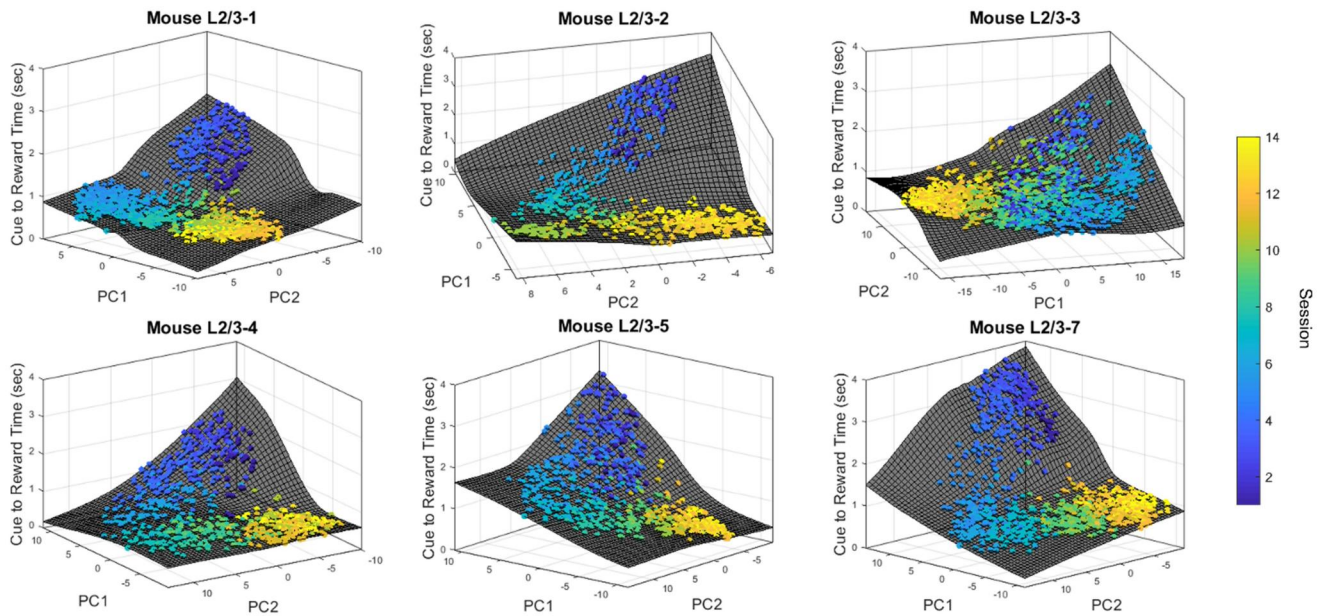
Figure 5. **L2/3 connectome activity versus cue-to-reward time for rewarded trials.** Each circle represents a rewarded trial and its color denotes the session number. The surface interpolation was done using MATLAB function cftool. The cue-to-reward time of each trial is projected onto the surface for visualization purposes.
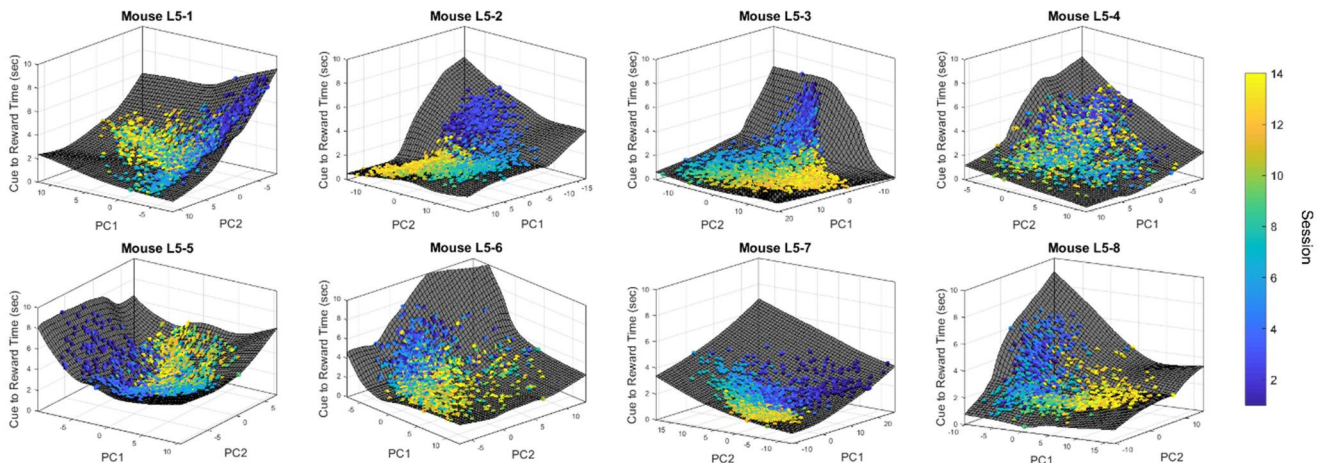
Figure 6. **L5 connectome activity versus cue-to-reward time for rewarded trials.** Each circle represents a rewarded trial and its color denotes the session number. The surface interpolation was done using MATLAB function `cftool`. The cue-to-reward time of each trial is projected onto the surface for visualization purposes.

Figure 7 compares the correlations for the first (Sessions 1–4) and the second phase (Sessions 5–14) for L2/3 and L5. The pseudotimes of L2/3 in the first phase of learning are negatively correlated with the cue-to-reward times (Figure 7a), suggesting that the learning-related trajectory here is associated with an improvement in motor performance. In comparison, the second phase of learning has markedly lower correlation (*i.e.* less negative). This trend agrees with the biphasic learning mentioned earlier. In contrast to L2/3, the pseudotimes of L5 show a mixture of positive and negative correlations (Figure 7b). That is, the association between the learning-related trajectory of L5 connectome activities and motor performance is weaker or less consistent than L2/3, in general agreement with the previous study (Peters et al. 2017).

3.3. Connectome Rewiring Revolves around a Core Set of Movement-Associated Neurons

The PCA findings above revealed insights related to alterations in the functional connectivity associated with learning. In the following, we focused on neurons in L2/3 that are most significantly impacted by motor learning. For this purpose, we identified functional connectivity edges that have the most highly positive and negative PC1 loadings of the connectome, as these reflect connectivity that is stably and significantly strengthened and weakened with learning, respectively (see Methods). From these edges, we obtained two groups of neurons: one group of neurons that are incident to the top positive PC1 connectivity edges and another incident to the top negative PC1 edges. Note that these groups are not mutually exclusive (*i.e.* there are neurons that belong to both groups). We analyzed the association of these neurons with lever movement by quantifying the fraction of movement-related neurons—defined as neurons that have significantly higher activity during movement epochs than during non-movement epochs (see Methods)—in each group. Specifically, we evaluated the fractions of neurons in each group that are movement-related in different learning

phases: session 1–2 (naïve), 3–5 (early), 6–9 (mid), and 10–14 (expert). As shown in Figure 8a, neurons from the top positive PC1 loading become more associated with movement with learning, while those from highly negative PC1 loadings do not exhibit a clear trend. As expected, L5 neurons associated with their respective top positive and negative PC1 loadings have weaker connection with movement than L2/3 neurons, as indicated by lower fractions of movement-related neurons (see Supplementary Figure 23).

In the following, we further subcategorized the two groups of neurons into three classes: Core, Naïve Phase (NP), and Expert Phase (EP). Core neurons are those associated with functional connectivity belonging to both top positive and negative PC1 loadings, and as such, they represent neurons that undergo the most extensive rewiring during motor learning (see Figure 8b and Supplementary Figure 26). EP (NP) neurons are associated exclusively with the top positive (negative) PC1 loadings, and they gain (lose) functional connectivity with learning. Neurons whose edges are not associated with top PC1 loadings are called other (O) neurons. Core neurons make up $35.68 \pm 3.30\%$ (mean $\pm$ s.e.m.) of L2/3 neurons. On the other hand, NP and EP neurons comprise $18.64 \pm 1.50\%$ and $24.67 \pm 1.65\%$ (mean $\pm$ s.e.m.) of the L2/3 neuronal population, respectively (see Figure 8c). Core neurons are more frequently movement related than all other groups of neurons over the learning period, as shown Figure 8d. Table 1 confirms that movement-related neurons are significantly overrepresented among Core neurons, but not the other classes of neurons. Meanwhile, NP (EP) neurons become less (more) movement-related with learning. Therefore, the neurons that are most extensively rewired during learning are strongly associated with movement.

Looking at the connectivity more closely, Core neurons maintain a relatively stable mean degree of connectivity across the learning sessions, as shown in Figure 9a, despite the fact that they are extensively rewired. This stability suggests that connectivity loss with learning is balanced by connectivity gain. Meanwhile, NP (EP) neurons show a decreasing (increasing) degree of connectivity with learning
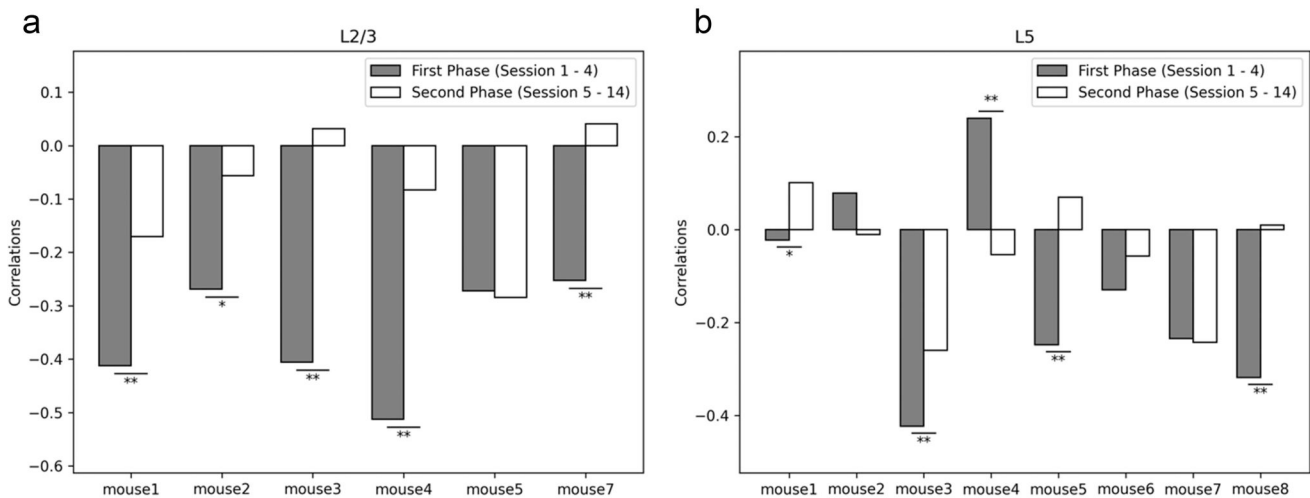
Figure 7. **Correlations between the cue-to-reward time and pseudotime**. Statistical significance was performed using two-sided two-sample t-test of Fisher z-transformed correlations (*: *p*-value < 0.05, **: *p*-value < 0.01).
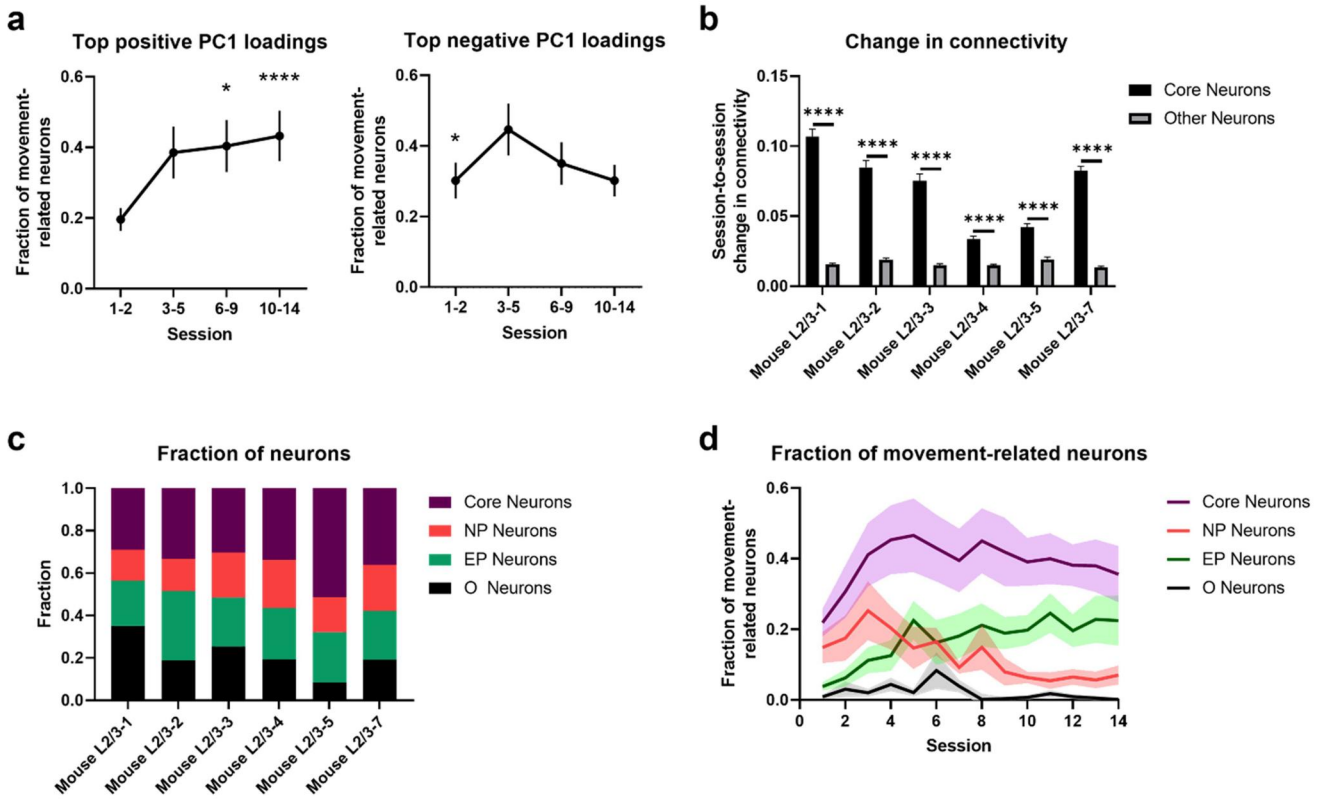
Figure 8. Analysis of top PC1 neurons in L2/3. **a.** Fractions of neurons from the top positive and the top negative PC1 loadings that are classified as movement related (* 5th upper percentile, ****0.01th upper percentile). **b.** Session-to-session connectivity change among core and non-core neurons. **** p-value $< 10^{-4}$ (two-sided two sample t-test). **c.** Fractions of core, NP, EP and O neurons ($n = 6$ mice). **d.** Fractions of movement-related neurons among core, NP, and EP groups. In all figures, shaded regions and error bars represent s.e.m. (**a** and **d**) across all animals or (**b**) across neurons for each animal.

Table 1. Over-representation of movement-related neurons in Core, NP, EP, and Other neurons in L2/3.

|	Session 1–2	Session 3–4	Session 6–9	Session 10–14
Core Neurons	4.569*	5.876*	5.773*	5.446*
NP Neurons	1.494	0.938	0.531	0.217
EP Neurons	0.221	0.461	0.715	1.314
O Neurons	0.129	0.102	0.105	0.077

The values indicate odds ratio. *p-value < 0.0001 (Fisher exact test).

(see Figure 9a). Figure 9b further shows that Core neurons have a higher intragroup than intergroup connectivity, i.e. Core neurons are connected mostly among themselves. In addition, Core neurons start with a higher connectivity with NP than EP neurons, but this is reversed over the course of learning where the loss of Core-NP connectivity is countered by the gain of Core-EP connectivity. This balancing between the strengthening and weakening of connectivity agrees with the observation that learning-induced rewiring in L2/3 maintains a homeostatic number of connectivity, and further reveal that the connectome rewiring concentrates on a core group of neurons that form highly connected sub-connectome with each other.

Next, we analyzed how motor-skill learning affects the activity of the different neuronal groups and its relationship with movements in rewarded trials. As shown in Figure 10a, Core neurons maintain a stable mean activity over the entire learning period that is relatively higher than the other groups of neurons (Figure 10a). NP and EP neurons follow an opposite trend in mean activity: a decrease for NP and an increase for EP (Figure 10a). The activity of Core and EP

neurons become more reproducible with learning, while NP and O neurons do not (Figure 10b). As described in the original study (Peters et al. 2014), learning leads to an emergence of reproducible neuronal activity in L2/3 and stereotyped movement, such that movements that are more similar to the stereotyped pattern are associated with neuronal activities that are also more similar to the learned activity pattern (Figure 3b in Peters et al. (Peters et al. 2014) and Figure 10c). Figure 10d–g shows that such learning-associated activity-movement relationship also emerges for the above groups of neurons, but it is the most prominent for Core neurons, followed by, in decreasing degree, EP, NP, and O neurons. Interestingly, even during the initial (naïve) phase of learning, the activity of Core neurons already resembles the learned activity pattern more closely when movements are highly correlated with the stereotyped expert pattern (movement correlation > 0.5), when compared with the other groups of neurons (see Figure 10h). The analysis above shows that Core neurons and their rewiring play a significant role in the emergence of stereotyped activity and movement patterns with motor-skill learning.

Finally, we investigated the differences across the groups of neurons in terms of encoding movement in their neuronal activity. To do so, for individual groups of neurons, we trained linear decoders that predict lever positions (lever voltages) from their neuronal activity (thresholded and smoothened spikes) for every session—called session decoders (see Methods). Figure 11a shows example test data of actual and predicted lever positions, while Figure 11b
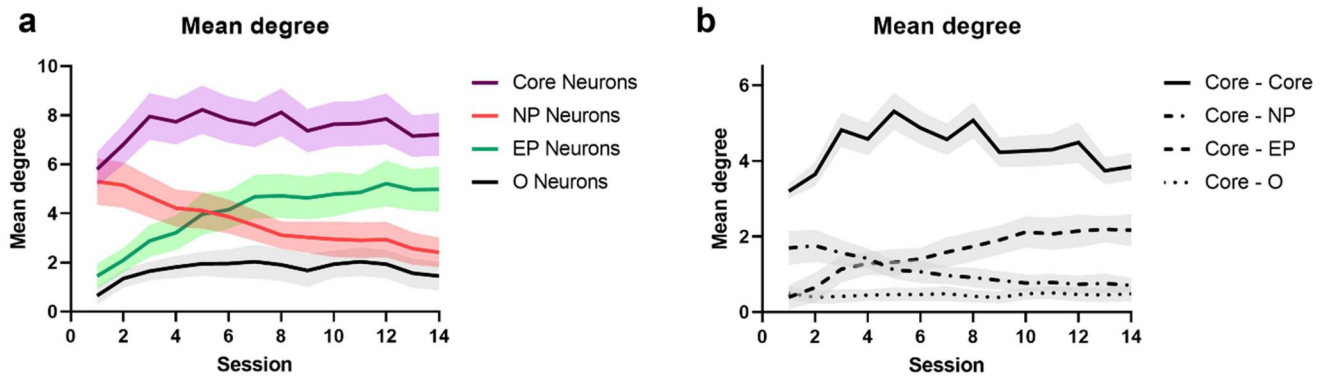
Figure 9. **Connectivity of top PC1 neurons. a.** Mean degree of connectivity. **b.** Mean degree connectivity of Core neurons with Core, NP, EP, and Other neurons. The shaded area denotes s.e.m. computed across all animals.

gives their correlations for the test data that were not used in the training of the decoders. Session decoders for Core neurons have the highest correlations, implying that Core neurons encode movements in their activity more strongly than the other groups of neurons. Besides, learning generally improves the accuracy of session decoders, indicating that there is an increase of movement-encoding within the neuronal activity of all groups of neurons in L2/3. The most significant learning-induced improvement is for EP neurons, followed by Core neurons, with only a small increase for NP and O neurons. We also tested the ability of linear decoders trained using data from the expert phase (session 10–14)—called expert decoders—to predict movements (lever positions) in the naïve phase (session 1–3). The correlations from these expert decoders are expectedly lower than using the respective session decoders (comparing Figure 11b and 11c). Still, expert decoders of Core neurons predict movements in the naïve phase significantly better than expert decoders of the other groups (p-value $< 10^{-10}$), and comparable to the session decoders from each respective group. This result points to the stability of movement encoding by Core neurons over the course of learning, suggesting that learning-related rewiring might be centered around producing a stable activity pattern in a core set of neurons that maintain reliable relationship with movements.

4. Discussion

The motor cortex plays a critical role in motor skill learning for integrating sensory information, establishing a motor plan, and executing movements (Li and Waters 1991; Pronichev and Lenkov 1998; Ferezou et al. 2007; Tennant et al. 2011; Guo et al. 2015; Li et al. 2016; Makino et al. 2016; Hwang et al. 2019a, 2019b; Sauerbrei et al. 2020). In previous studies, lever-press task learning has been associated with the reorganization of neuronal population activity in L2/3 and L5 of the mouse M1, as measured by *in vivo* two-photon calcium imaging. In L2/3 neurons, consistent spatiotemporal population activity emerges accompanying learned movements (see Figure 2c), leading to a stronger correlation between movement similarity and neuronal activity similarity (Peters et al. 2014). In L5, despite the same motor learning as L2/3, no consistent neuronal population

activity was observed (see Figure 2d), but instead dissimilar movements became further decorrelated (Peters et al. 2017). The contrasting learning-induced reorganizations of neuronal activity across different layers in the primary motor cortex suggest differences in their roles and functional objectives during motor learning (Peters et al. 2014, 2017).

Interestingly, despite the overt differences in how lever-press task learning affects the neuronal population activities in L2/3 and L5, their functional connectomes—as measured by partial correlations of calcium spikes—show similar rewiring trajectories (see Figure 3 & 4). Specifically, our analysis shows that the functional connectomes in both layers rewire to become more interconnected during the first few learning sessions (Sessions 1–4), whereby the statistical dependencies of neuronal activities strengthen. In the later sessions, functional connections are gradually pruned, reflecting weakening correlations of neuronal activities. This result agrees well with a transient increase of L2/3 spine density measured in mice undergoing the same motor task learning, suggesting that changes of the functional connectivity in L2/3 are connected, at least partly, to learning-related plasticity of dendritic spines (Peters et al. 2014).

Meanwhile, the rewiring in L5 functional connectomes is associated with more subdued and delayed changes in network interconnectedness when compared to L2/3 functional connectomes: L5 peaking at around the 7th learning session vs. L2/3 peaking at roughly the 3rd learning session (see Figures 3d and 4d). While it is known that L2/3 neurons project to L5, the lack of coherence in learning-induced changes of neuronal activity patterns and the differences in magnitude and speed of rewiring dynamics between the two layers suggest a weak inter-layer coordination of neuronal communications. That is, while the functional connectome rewiring in L2/3 and L5 occurs relatively independently of each other, both appear to engage the same rewiring principle.

Our analysis further strengthens the overt connection between spatiotemporal neuronal population activity in L2/3 and lever movement. By quantifying the functional connectome activity on a trial-to-trial basis, we demonstrated a strong correlation between functional connectome activity changes across trials with improved motor performance, as measured by the cue-to-reward time, in the early learning
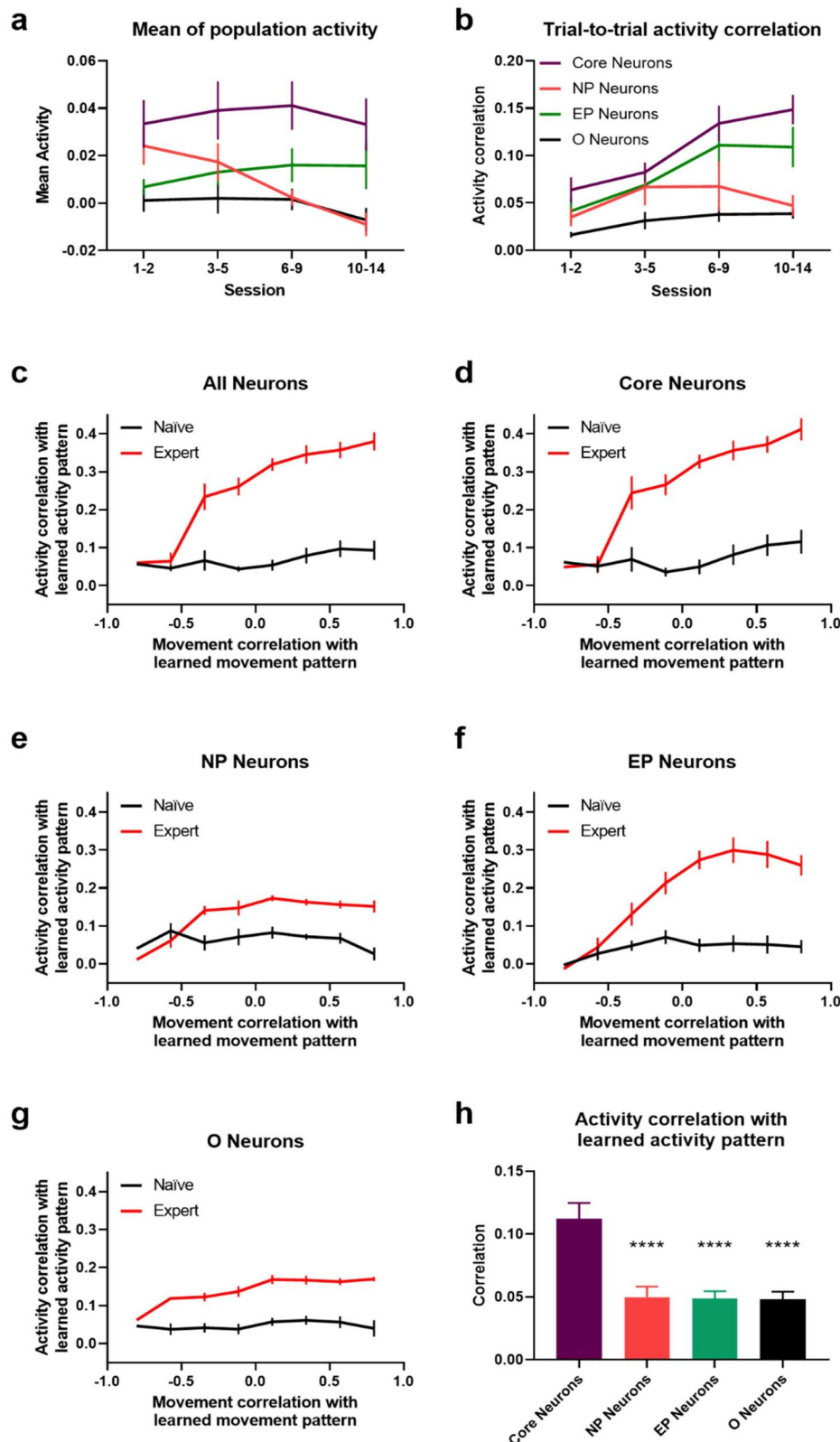
Figure 10. **Neuronal activity and movement encoding. a.** Mean neuronal activity of different groups in learning trials. **b.** Trial-to-trial activity correlation for different groups of neurons. (**c–g**) Correlations of activity vs. movement with respective expert patterns in cued trials (84-frame window) for all (**c**), Core (**d**), NP (**e**), EP neurons (**f**), and Other neurons (**g**). Naïve refers to session 1-3 and expert to session 10-14. **h.** Neuronal activity correlation with learned pattern for expert-like movements (corr. > 0.5) in naïve sessions. **** p-value < 0.0001 (one-sided paired t-test). Error bars indicate s.e.m computed across all L2/3 animals.

sessions (Sessions 1–4, see Figures 5 and 7). This period coincides with a sharp increase in the interconnectedness of the functional connectome. Thus, L2/3 functional connectomes appear to initially adopt higher interconnectivity

when optimizing for motor performance. In the second half of the experiments (session 8–14), functional connectomes and their activities continue to rewire, where functional connectivity is gradually pruned, even after the cue-to-reward
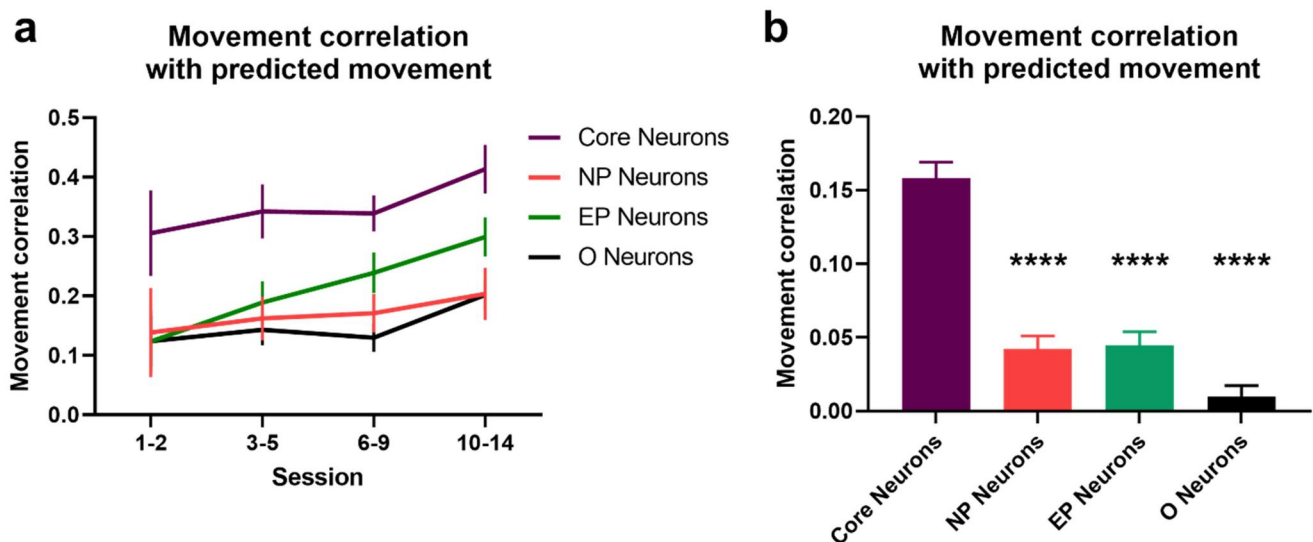
Figure 11. Encoding of movement in neuronal activity *via* **linear decoders. a.** Correlations between actual and predicted movement based on linear decoders built for each session and used to predict movements of the unseen trials of the same session. **b.** Correlations between actual and predicted movement for naïve sessions (session 1-3) using a linear decoder trained using data from expert sessions (session 10–14). **** *p*-value < 0.0001 (two-sided two-sample t-test). Error bars indicate s.e.m computed across animals.

time reaches a plateau. On the other hand, the correlation between the changes in the functional connectome activity and motor performance is visibly less prominent in L5 when compared with L2/3 (Figures. 6 and 7).

The results of these analyses suggest that a common rewiring dynamics underpin learning-induced changes in L2/3 and L5 in the mouse primary motor cortex. The overlap of time periods when L2/3 functional connectomes sharply increase their degrees of connectivity and when the cue-to-reward times markedly improve, suggests that higher interconnectedness has a functional relevance in terms of motor performance. The overt higher level of connectivity in the functional connectomes is consistent with an exploration of network state space—the space of network structures—to optimize a learning-related functional objective. Once the learning-related objective reaches an optimal (desirable) level, the functional connectome rewiring dynamics engages a different trajectory to return to homeostatic level of network connectivity and presumably a network state with high energetic efficiency. Thus, functional connectome rewiring appears to be driven by multiple objectives, where the dominant objective switches from one to another across learning and/or these objectives have large time-scale separation.

Further analyses focused on L2/3 neurons whose functional connectivity are most significantly altered by learning—*i.e.* neurons associated with the shift along the PC1 scores between naïve and expert sessions in Figure 3. The analyses showed how learning-induced rewiring clusters around a core set of movement-associated neurons (Core neurons). Core neurons form a highly interconnected hub in the connectome where these neurons are highly interconnected among each other. Learning heavily adds and removes connectivity among these neurons, but in a manner that maintains the overall degree of connectivity, i.e. losses of connectivity are balanced by gains. Further, Core neurons reliably encode movements in response to cues even in the

naïve phase, and learning-associated rewiring further improves their movement encoding. Beside the aforesaid Core neurons, there are also neurons that steadily gain and lose connectivity with learning, i.e. EP and NP neurons, respectively. While the gain of connectivity among EP neurons is associated with increased association of their activity with movement, the loss of connectivity among NP neurons does not significantly affect their activity-movement relationship. These distinct patterns of connectivity changes among the three different neuronal groups and their relationship to movements suggest that motor learning is accompanied by neuronal rewiring that reinforces the activity pattern of Core neurons that reliably encode the learned movement.

There are important limitations to the present study. First and foremost, this study adopted a fully data-driven approach using statistical dependencies of neuronal activities to inform on the reorganizations of functional connectivity among neurons in L2/3 and L5 of the M1 during motor skill learning. While such learning-related changes may arise from the physical formation and loss of synaptic connections among these neurons—as indicated by the previously reported rise-then-fall dynamics of synaptic bouton density in L2/3 during the same motor learning (Peters et al. 2014)—they may also come from other sources, for example alterations in the input signals to the M1 from other brain regions such as parietal, premotor, and frontal cortices, as well as the somatosensory cortex (Mateer and Sira 2003). Also, because partial correlations are symmetric, the identity of the pre- and post-synaptic neurons is missing. The lack of such information prevents more detailed insights into the organizational principles of motor learning (e.g. changes in the proportion of pre- and post-synaptic neurons). Lastly, the study focused on a 14-session (2-week) learning period. Long term studies of motor learning (1–2 months) have shown the disengagement of M1 from movement control while animals maintain the learned movements (Hwang

et al. 2019a, 2021). This observation suggests that connectome reorganization in motor learning continues beyond the period of this study and involves other brain region(s) besides the M1.

5. Conclusion

In lever-press task learning, distinct reorganizations of neuronal activity occur in the L2/3 and L5 of M1, reflecting different roles and functional objectives across layers during motor learning. However, the analysis of functional connectomes over the learning sessions, reconstructed from neuronal activities using partial correlations, reveals similar rewiring trajectories in L2/3 and L5. Specifically, increased functional interconnectivity (stronger coordination of neuronal firing) during the early phase of learning, followed by connectivity pruning in the later sessions, highlights the shared principle of rewiring between L2/3 and L5 of M1. Further, the reorganization of connectome activity in L2/3, but not L5, during the early learning phase overlaps with marked improvement of the motor performance, suggesting the functional relevance of higher interconnectivity in L2/3 for motor optimization. In the later phase, the rewiring dynamics appear to favor a return to a homeostatic level of network connectivity, indicating a shift in the rewiring objective. Lastly, learning-induced rewiring particularly impacts a core set of movement-associated neurons in L2/3, and this reinforces the activity patterns that encode the learned movement. Overall, this study significantly enhances our understanding of the functional connectome rewiring dynamics during motor learning.

Acknowledgement

Disclosure statement

No potential conflict of interest was reported by the author(s).

ORCID

Saber Meamardoost (iD) http://orcid.org/0000-0002-9491-457X
Mahasweta Bhattacharya (iD) http://orcid.org/0000-0001-9653-2893
Eun Jung Hwang (iD) http://orcid.org/0000-0003-2786-5963
Chi Ren (iD) http://orcid.org/0000-0002-0947-8516
Linbing Wang (iD) http://orcid.org/0000-0003-2670-376X
Ying Zhang (iD) http://orcid.org/0000-0001-8654-7135
Takaki Komiyama (iD) http://orcid.org/0000-0001-9609-4600
Rudiyanto Gunawan (iD) http://orcid.org/0000-0002-6480-7976

Data availability statement

Functional connectomes and MATLAB and Python codes used in this study are available at https://github.com/CABSEL/Connectome-Rewiring. The method FARCI is available at https://github.com/CABSEL/FARCI.

References

Albarran E, Raissi A, Jáidar O, Shatz CJ, Ding JB. 2021. Enhancing motor learning by increasing the stability of newly formed dendritic spines in the motor cortex. Neuron. 109(20):3298–3311.e4. doi:10.1016/j.neuron.2021.07.030

Anon 1987. Multidimensional scaling: history, theory, and applications. Hillsdale, NJ, US: Lawrence Erlbaum Associates, Inc.

Bassett DS, Wymbs NF, Porter MA, Mucha PJ, Carlson JM, Grafton ST. 2011. Dynamic reconfiguration of human brain networks during learning. Proc Natl Acad Sci U S A. 108(18):7641–7646. doi:10.1073/pnas.1018985108

Bathe M, Hernandez R, Komiyama T, Machiraju R, Neogi S. 2021. Autonomous computing materials. ACS Nano. 15(3):3586–3592. doi:10.1021/acsnano.0c09556

Bennett SH, Kirby AJ, Finnerty GT. 2018. Rewiring the connectome: evidence and effects. Neurosci Biobehav Rev. 88:51–62. doi:10.1016/j.neubiorev.2018.03.001. PMID: 29540321.

Caroni P, Donato F, Muller D. 2012. Structural plasticity upon learning: regulation and functions. Nat Rev Neurosci. 13:478–490. doi:10.1038/nrn3258

Citri A, Malenka RC. 2008. Synaptic Plasticity: multiple forms, functions, and mechanisms. Neuropsychopharmacology. 33(1):18–41. doi:10.1038/sj.npp.1301559

Ferezou I, Haiss F, Gentet LJ, Aronoff R, Weber B, Petersen CCH. 2007. Spatiotemporal dynamics of cortical sensorimotor integration in behaving mice. Neuron. 56(5):907–923. doi:10.1016/j.neuron.2007.10.007

Fisher RA. 1921. On the probable error of a coefficient of correlation deduced from a small sample. Available at: https://www.scinapse.io/papers/404240460. [Accessed June 17, 2023].

Friedrich J, Zhou P, Paninski L. 2017. Fast online deconvolution of calcium imaging data. PLoS Comput Biol. 13(3):e1005423. doi:10.1371/journal.pcbi.1005423

Fu M, Yu X, Lu J, Zuo Y. 2012. Repetitive motor learning induces coordinated formation of clustered dendritic spines in vivo. Nature. 483(7387):92–95. doi:10.1038/nature10844

Greenough WT, Larson JR, Withers GS. 1985. Effects of unilateral and bilateral training in a reaching task on dendritic branching of neurons in the rat motor-sensory forelimb cortex. Behav Neural Biol. 44(2):301–314. doi:10.1016/S0163-1047(85)90310-3

Guo JZ, Graves AR, Guo WW, Zheng J, Lee A, Rodríguez-Gonzá Lez J, Li N, Macklin JJ, Phillips JW, Mensh BD, Branson K, et al. 2015. Cortex commands the performance of skilled movement. eLife. 4:e10774. doi:10.7554/eLife.10774

Haghverdi L, Büttner M, Wolf FA, Buettner F, Theis FJ. 2016. Diffusion pseudotime robustly reconstructs lineage branching. Nat Methods. 13(10):845–848. doi:10.1038/nmeth.3971

Huang L, Zhou H, Chen K, Chen X, Yang G. 2020. Learning-dependent dendritic spine plasticity is reduced in the aged mouse cortex. Front Neural Circuits. 14:581435. Available at: https://www.frontiersin.org/article/10.3389/fncir.2020.581435. [Accessed February 7, 2022]. doi:10.3389/fncir.2020.581435

Hwang EJ, Dahlen JE, Hu YY, Aguilar K, Yu B, Mukundan M, Mitani A, Komiyama T. 2019a. Disengagement of motor cortex from movement control during long-term learning. Sci Adv. 5(10):eaay0001. doi:10.1126/sciadv.aay0001

Hwang EJ, Dahlen JE, Mukundan M, Komiyama T. 2021. Disengagement of motor cortex during long-term learning tracks the performance level of learned movements. J Neurosci. 41(33):7029–7047. doi:10.1523/JNEUROSCI.3049-20.2021

Hwang EJ, Link TD, Hu YY, Lu S, Wang EH-J, Lilascharoen V, Aronson S, O'Neil K, Lim BK, Komiyama T. 2019b. Corticostriatal flow of action selection bias. Neuron. 104(6):1126–1140.e6. doi:10.1016/j.neuron.2019.09.028

Kao CH, Khambhati AN, Bassett DS, Nassar MR, McGuire JT, Gold JI, Kable JW. 2020. Functional brain network reconfiguration during learning in a dynamic environment. Nat Commun. 11(1):1682. doi:10.1038/s41467-020-15442-2

Lee C, Kim Y, Kaang B-K. 2022. The primary motor cortex: the hub of motor learning in rodents. Neuroscience. 485:163–170. Available at: https://www.sciencedirect.com/science/article/pii/S0306452222000161. [Accessed February 5, 2022]. doi:10.1016/j.neuroscience.2022.01.009

Li CX, Waters RS. 1991. Organization of the mouse motor cortex studied by retrograde tracing and intracortical microstimulation (ICMS) mapping. Can J Neurol Sci. 18(1):28–38. doi:10.1017/S0317167100031267

Li N, Daie K, Svoboda K, Druckmann S. 2016. Robust neuronal dynamics in premotor cortex during motor planning. Nature. 532(7600):459–464. doi:10.1038/nature17643

Makino H, Hwang EJ, Hedrick NG, Komiyama T. 2016. Circuit mechanisms of sensorimotor learning. Neuron. 92(4):705–721. doi:10.1016/j.neuron.2016.10.029

Mateer CA, Sira CS. 2003. Executive Function. In: Aminoff MJ, Daroff RB, editors. Encyclopedia of the Neurological Sciences,. New York: Academic Press. p. 317–320 Available at: https://www.sciencedirect.com/science/article/pii/B0122268709007401. [Accessed June 17, 2023].

McInnes L, Healy J, Melville J. 2020. UMAP: uniform manifold approximation and projection for dimension reduction. ArXiv180203426 Cs Stat Available at: http://arxiv.org/abs/1802.03426. [Accessed February 21, 2022].

Meamardoost S, Bhattacharya M, Hwang EJ, Komiyama T, Mewes C, Wang L, Zhang Y, Gunawan R. 2021. FARCI: fast and robust connectome inference. Brain Sci. 11(12):1556. doi:10.3390/brainsci11121556

Muñoz-Castañeda R, Zingg B, Matho KS, Chen X, Wang Q, Foster NN, Li A, Narasimhan A, Hirokawa KE, Huo B, et al. 2021. Cellular anatomy of the mouse primary motor cortex. Nature. 598:159–166. doi:10.1038/s41586-021-03970-w

Pachitariu M, Stringer C, Harris KD. 2018. Robustness of spike deconvolution for neuronal calcium imaging. J Neurosci. 38(37):7976–7985. doi:10.1523/JNEUROSCI.3339-17.2018. PMID: 30082416.

Papale AE, Hooks BM. 2018. Circuit changes in motor cortex during motor skill learning. Neuroscience. 368:283–297. doi:10.1016/j.neuroscience.2017.09.010

Peters AJ, Chen SX, Komiyama T. 2014. Emergence of reproducible spatiotemporal activity during motor learning. Nature. 510(7504):263–267. doi:10.1038/nature13235

Peters AJ, Lee J, Hedrick NG, O'Neil K, Komiyama T. 2017. Reorganization of corticospinal output during motor learning. Nat Neurosci. 20(8):1133–1141. doi:10.1038/nn.4596

Pronichev IV, Lenkov DN. 1998. Functional mapping of the motor cortex of the white mouse by a microstimulation method. Neurosci Behav Physiol. 28(1):80–85. doi:10.1007/BF02461916

Satopaa V, Albrecht J, Irwin D, Raghavan B. 2011. Finding a "Kneedle" in a haystack: detecting knee points in system behavior. In: 2011 31st International Conference on Distributed Computing Systems Workshops; 2011 June 20–24; Minneapolis, MN. Los Alamitos, CA: IEEE Computer Society. p. 166–171. doi:10.1109/ICDCSW.2011.20.

Sauerbrei BA, Guo JZ, Cohen JD, Mischiati M, Guo W, Kabra M, Verma N, Mensh B, Branson K, Hantman AW. 2020. Cortical pattern generation during dexterous movement is input-driven. Nature. 577(7790):386–391. doi:10.1038/s41586-019-1869-9

Stosiek C, Garaschuk O, Holthoff K, Konnerth A. 2003. In vivo two-photon calcium imaging of neuronal networks. Proc Natl Acad Sci U S A. 100(12):7319–7324. doi:10.1073/pnas.1232232100

Tennant KA, Adkins DL, Donlan NA, Asay AL, Thomas N, Kleim JA, Jones TA. 2011. The organization of the forelimb representation of the C57BL/6 mouse motor cortex as defined by intracortical microstimulation and cytoarchitecture. Cereb Cortex. 21(4):865–876. doi:10.1093/cercor/bhq159

Wang L, Conner JM, Rickert J, Tuszynski MH. 2011. Structural plasticity within highly specific neuronal populations identifies a unique parcellation of motor learning in the adult brain. Proc Natl Acad Sci U S A. 108(6):2545–2550. doi:10.1073/pnas.1014335108

Withers GS, Greenough WT. 1989. Reach training selectively alters dendritic branching in subpopulations of layer IIII pyramids in rat motor-somatosensory forelimb cortex. Neuropsychologia. 27(1):61–69. doi:10.1016/0028-3932(89)90090-0

Wolf FA, Angerer P, Theis FJ. 2018. SCANPY: large-scale single-cell gene expression data analysis. Genome Biol. 19(1):15. doi:10.1186/s13059-017-1382-0

Xu T, Yu X, Perlik AJ, Tobin WF, Zweig JA, Tennant K, Jones T, Zuo Y. 2009. Rapid formation and selective stabilization of synapses for enduring motor memories. Nature. 462(7275):915–919. doi:10.1038/nature08389

Yang G, Pan F, Gan W-B. 2009. Stably maintained dendritic spines are associated with lifelong memories. Nature. 462(7275):920–924. doi:10.1038/nature08577